Emergency Lane-Change Maneuvers of Autonomous Vehicles

Zvi Shiller
Department of Mechanical and Aerospace Engineering, University of California Los Angeles, Los Angeles, CA 90095-1597

Satish Sundar
Applied Materials Inc., Santa Clara, CA 95054

This paper addresses the issue of collision avoidance using lane-change maneuvers. Of particular interest is to determine the minimum distance beyond which an obstacle cannot be avoided at a given initial speed. Using a planar bicycle model, we first compute the sharpest dynamically feasible maneuver by minimizing the longitudinal distance of a lane transition, assuming given initial and free final speeds. The minimum distance to an obstacle is then determined from the path traced by the optimal maneuver. Plotting the minimum distance in the phase plane establishes the clearance curve, a valuable tool for planning emergency maneuvers. For the bicycle model, the clearance curve is shown to closely correlate with the straight line produced by a point mass model. Examples demonstrate the use of the clearance curve for planning safe avoidance maneuvers.

1 Introduction

Collision avoidance represents a central safety issue for automated vehicles. It concerns the avoidance of static obstacles, such as disabled vehicles, and large objects blocking the forward path. Collision can be avoided either by decelerating to a full stop without hitting the obstacle, or by executing a timely lane-change maneuver. A lane-change maneuver is generally more desirable since it least disturbs the traffic flow. However, executing a lane-change maneuver may depend on the traffic in the neighboring lanes, vehicle speed, and its distance to the obstacle. This can be demonstrated with the following scenario. An obstacle is detected in the forward path. If the traffic in the neighboring lane allows a lane change, then the vehicle may execute a comfortable lane transition, using for example the method presented in Chee and Tomizuka (1994). However, if the traffic in the neighboring lane does not allow a lane change, and the distance and speed are insufficient for a full stop, then the vehicle may slow down in the current lane, hoping for a space to open in the neighboring lanes. At some point, as the vehicle approaches the obstacle, a lane change may no longer be feasible. This is the point beyond which any lane change maneuver would result in an off-center collision. Determining the states (position and speed) beyond which a lane change maneuver is infeasible as a function of vehicle dynamics is the main focus of this paper.

To determine the last point for a lane transition, we solve the inverse problem: first compute the optimal maneuver that minimizes the longitudinal displacement of the lane transition, assuming given initial and free final speeds, then determine the distance to the closest obstacle avoidable by this maneuver. The optimal maneuver is the sharpest feasible at given speed, vehicle dynamics, and road conditions. We call it an emergency maneuver since it minimizes the reaction time and the reaction distance while reaching the vehicle's performance limits.

Plotting the minimum distance in the phase plane (speed versus distance from obstacle) produces what we call the clearance curve, which divides the phase plane into two regions: states right of the curve are *avoidable* (an obstacle is avoidable by some lane-change maneuver from these states), whereas states left of the curve would result in collision. States along the curve are avoidable by the optimal maneuvers only. The clearance curve thus provides a valuable decision tool for planning safe avoidance maneuvers, as is demonstrated in this paper. Clearly, the farther the initial state to the right of the clearance curve, the more comfortable the maneuver. The computation of "comfortable" maneuvers (satisfying "comfort" related criteria such as acceleration and jerk constraints) has been treated elsewhere (Chee and Tomizuka, 1994) and is out of the scope of this paper.

We resort to simple vehicle models (the simpler the better) to allow fast on-line computation, consistent with emergency situations. We first use a front steering planar bicycle model, with the steering angle and the rear tractive force as the two control variables. The computation of the optimal maneuvers is formulated as a parameter optimization over parameters representing the vehicle's trajectory. This formulation requires solving the inverse dynamics problem, which for the bicycle model and the tire model used is computationally feasible. Higher-order vehicle dynamics and a more detailed tire model would have made this optimization computationally very difficult. Optimizing instead over the control inputs (using the Pontryagin Maximum Principle) is generally more difficult due to the additional co-states (Lagrange multipliers).

The clearance curve is determined from optimal trajectories computed for various initial speeds. For on-line generation of the clearance curve, we propose to approximate the optimal maneuvers using a simple point mass model. Despite its simplicity, the point mass model is shown to produce optimal paths that closely correlate with the optimal paths computed for the planar vehicle model. The clearance curves produced by both models are therefore almost identical.

This should not imply that the linear point mass model is a substitute for the more accurate nonlinear bicycle model in computing emergency maneuvers. It is not. While the paths generated by both models are very similar, their velocity profiles are not. Nevertheless, the point mass model is useful for on-line approximations of the clearance curve, and with proper selection of the model parameters, for on-line generation of conservative emergency lane-change maneuvers.

The problem of emergency maneuvers has been little addressed in the literature to date. Smith and Starkey (1994) generated emergency maneuvers at 110 km/h over a 60 m lane transition by optimizing the gains of a linear controller over the step response of the nonlinear vehicle model. Their assumption of constant speeds (lateral control only) resulted in maneuvers

Contributed by the Dynamic Systems and Control Division for publication in the JOURNAL OF DYNAMIC SYSTEMS, MEASUREMENT, AND CONTROL. Manuscript received by the DSCD February 15, 1996. Associate Technical Editor: S. D. Fassois.

longer than necessary. Obstacle avoidance has been addressed experimentally in Fujita et al. (1994). Their results are remarkably similar to ours, as is discussed later in this paper.

Related work, but not directly addressing emergency maneuvers, is by Nerandran and Hedrick (1993) who developed a nonlinear controller for lane change maneuvers of a combined lateral and longitudinal vehicle model. However, this controller was tested in numerical simulations at moderate speeds only. In Chee and Tomizuka (1994), lane-change maneuvers at high speeds (110 km/h) were generated, using a lateral controller and assuming a constant longitudinal speed. The assumption of constant speed and constraints on the acceleration and jerk resulted in rather long maneuvers, lasting 6 s over 180 m, compared to less than 2.5 s (regardless of speed) and 80 m (for the same speed) for the maneuvers presented in this paper. An on-line method for planning maneuvers to account for traffic in the neighboring lanes was presented in Fiorini and Shiller (1998).

In this paper, we first present in Section 2 the planar bicycle model. Section 3 presents the tire model and the friction ellipse. Section 4 presents the problem formulation and computation of optimal lane-change maneuvers. In Section 5, these maneuvers are used to produce the clearance curve. Section 6 addresses the issue of on-line computation of emergency maneuver and the clearance curve. Section 7 presents examples of optimal and approximated maneuvers for the planar bicycle model.

2 Vehicle Model

The vehicle is modeled as the planar bicycle shown in Fig. 1. The absolute orientation of the vehicle in the inertial frame is φ; the angle of the linear velocity of its mass center is θ; and the steering angle of the front wheel is β. The orientation of the rear wheel is fixed relative to the vehicle.

The angles between the linear velocities of the rear and front wheels and their major axes are the rear and front slip angles, α_r and α_f, respectively. Both can be derived as functions of the vehicle's states (Shiller and Sundar, 1995):

$$\alpha_r = \tan^{-1}\left[\frac{-d_r\dot{\varphi} + \dot{y}\cos\varphi - \dot{x}\sin\varphi}{\dot{x}\cos\varphi + \dot{y}\sin\varphi}\right] \tag{1}$$

$$\alpha_f = \tan^{-1}\left[\frac{d_f\dot{\varphi} + \dot{y}\cos\varphi - \dot{x}\sin\varphi}{\dot{x}\cos\varphi + \dot{y}\sin\varphi}\right] - \beta \tag{2}$$

where $\dot{x}$ and $\dot{y}$ represent the velocity of the mass center in the inertial frame, and d_r and d_f are the length of the vehicle between the mass center and the centers of the rear and front wheels, respectively.

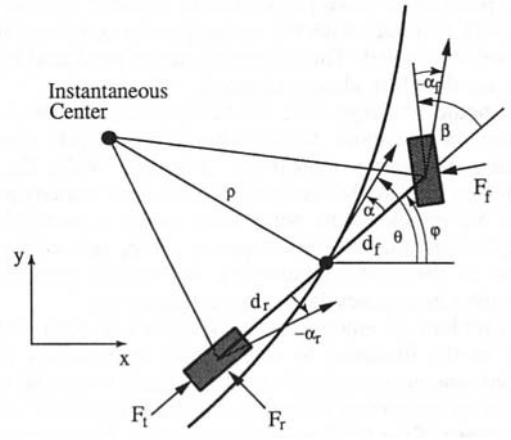

Fig. 1 The bicycle model

The external forces acting on the vehicle consist of a side force, F_r, and a longitudinal force, F_t, generated by the rear tire, and a side force, F_f, generated by the front tire. The force F_t, due to the engine torque or brakes, is one of the two control inputs, and is called the tractive force.

The equations of motion in the inertial frame are:

$$F_t\cos\varphi - F_r\sin\varphi - F_f\sin(\varphi+\beta) = m\ddot{x} \tag{3}$$

$$F_t\sin\varphi + F_r\cos\varphi + F_f\cos(\varphi+\beta) = m\ddot{y} \tag{4}$$

$$-d_rF_r + d_fF_f\cos\beta = I\ddot{\varphi} \tag{5}$$

where m is the vehicle mass, and I is its moment of inertia around the mass center.

Clearly, $\ddot{\varphi}$, cannot be arbitrarily specified, since F_r and F_f are state dependent. The moment equation (5) is, therefore, an equality constraint that eliminates one of the vehicle's three degrees-of-freedom.

3 Tire Model

The forces generated between the tire and ground are typically represented in the tire coordinate frame by a longitudinal and a lateral force, as was shown for the rear tire in Fig. 1. We have studied several tire models, including those developed by Dugoff (1970) and Sakai (1981). The Dugoff model is empirical, providing analytical relations for the longitudinal and lateral forces as functions of the slip angle and slip ratio. It accounts for the coupling between the side and longitudinal forces, known as the *friction ellipse*.

The Sakai model is theoretical, based on modeling of the tire/road interaction (Sakai, 1981). The longitudinal and side forces computed by this model are coupled by elliptical curves which better approximate the experimental data than the Dugoff model (Maalej et al., 1989). However, the Dugoff model is simpler, and its friction ellipse easier to compute. In addition, the Dugoff model *underestimates* the actual tire forces (Maalej et al., 1989), which might be suitable for computing safe (conservative) emergency maneuvers.

The empirical Dugoff model for a typical tire is (Dugoff et al., 1970):

$$F_x = -\frac{C_s s}{1-s} f(\lambda) \tag{6}$$

$$F_y = -\frac{C_\alpha \tan\alpha}{1-s} f(\lambda) \tag{7}$$

where

$$\lambda = \frac{\mu W(1-\epsilon v\sqrt{s^2+\tan^2\alpha})(1-s)}{2\sqrt{c_s^2s^2 + C_\alpha^2\tan^2\alpha}} \tag{8}$$

$$f(\lambda) = \begin{cases} \lambda(2-\lambda) & \text{for } \lambda < 1 \\ 1 & \text{for } \lambda > 1 \end{cases} \tag{9}$$

F_x is the longitudinal force, F_y is the side force, s is the longitudinal slip, α is the tire slip angle, C_s is the longitudinal stiffness, C_α is the cornering stiffens, W is the vertical load, v is the vehicle speed, μ is the coefficient of road adhesion, and ϵ is the adhesion reduction coefficient. Note that the vertical load, W, is constant due to the assumption of a planar bicycle model. In the bicycle model, F_f corresponds to F_y of the front wheel, F_r to F_y of the real wheel, and F_t to F_x of the rear wheel. F_x of the front wheel is zero as wheel dynamics are ignored.

The coupling between the side and longitudinal forces is a function of the slip angle, as shown in Fig. 2 for fixed tire parameters. The curves shown in Fig. 2 can be approximated by ellipses, with major axes dependent on the slip angle:

$$\left(\frac{F_x}{F_{x\max}(\alpha)}\right)^2 + \left(\frac{F_y}{F_{y\max}(\alpha)}\right)^2 = 1 \tag{10}$$

$F_{y\max}$ is computed by setting the slip ratio $s = 0$ in (7):

$$F_y = -C_\alpha \tan \alpha f(\lambda) \tag{11}$$

where

$$\lambda = \frac{\mu W(1 - \epsilon v \tan \alpha)}{2C_\alpha \tan \alpha} \tag{12}$$

and $F_{x\max}$ is computed by:

$$F_{x\max}(\alpha) = \lim_{s\to 1} F_x = \frac{C_s \mu W(1 - \epsilon v\sqrt{1 + \tan^2 \alpha})}{\sqrt{C_s^2 + C_\alpha^2 \tan^2 \alpha}} \tag{13}$$

Using this tire model would severely couple the equations of motion, making the optimization problem difficult to solve. For simplicity, we consider only the linear portion of the lateral tire force (see Gim and Nikravesh, 1991, for experimental data), modeling it by the linear function

$$F_y = -C_\alpha \alpha, \quad |\alpha| < \alpha^* \tag{14}$$

where α^* corresponds to the upper limit of the linear range (typically between 5 to 10 deg). Note that the side force varies little from 5 to 10 deg, as shown in Fig. 2. It is therefore safer to select $\alpha^* = 5$ deg, with only a small degredation in performance.

The friction ellipse (10) is relevant for the rear wheel only since the front wheel is assumed to spin freely, and thus generate only a side force according to (7). For the rear wheel, we treat F_t, the tractive force, as the control input, independent of the rear slip angle (the slip should be whatever is necessary to generate the specified force). Both F_t and F_r (the side force of the real wheel) are determined by inverse dynamics for a given trajectory. To account for the coupling between F_t and F_r, we bound the vector sum of the tractive and the side forces by the friction ellipse:

$$\left(\frac{F_t}{F_{x\max}}\right)^2 + \left(\frac{F_r}{F^*_{y\max}}\right)^2 \le 1 \tag{15}$$

where $F_{x\max}$ is computed using (13), and $F^*_{y\max}$ is computed using (11) by setting $\alpha = \alpha^*$. This constraint serves later as a state dependent control constraint on F_t (F_r is a state dependent force).

Properly choosing α^* would ensure that $F_r, F_f < F_{y\max}$. However, this is not essential as the state and control constraints introduced later ensure that the side forces of both wheels stay below $F_{y\max}$.

Limiting α to the range $[-\alpha^*, \alpha^*]$ does not utilize the full range of the tire forces, which in turn may result in conservative maneuvers that do not fully exploit the vehicle's dynamic performance. This may be necessary to ensure safety since operating near tire saturation is dangerous due to the high uncertainty of the tire/road parameters. The trajectories computed using this tire model might therefore represent the performance of the average driver, rather than of the expert driver. Such trajectories can, however, be used as reference inputs to on-line feedback controllers (lateral and longitudinal), or to provide insights into the general shape of limiting lane-change maneuvers. They do not by any means indicate the true performance limit of the vehicle. To compute such limiting trajectories would require to further study tire performance near saturation, and to experimentally tune the parameters of the tire model, both out of the scope of this paper.

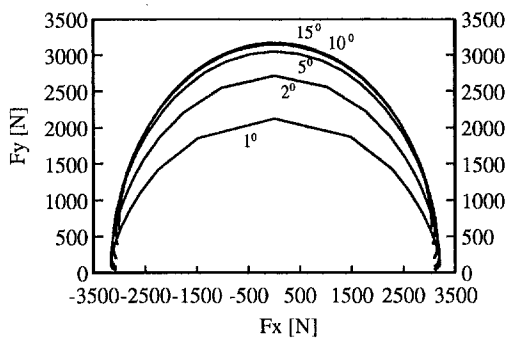

Fig. 2 The Dugoff model

4 Emergency Lane-Change Maneuver

A typical emergency lane-change maneuver is shown in Fig. 3, where a vehicle, moving at some initial speed, $\dot{x}_0$, avoids an obstacle that is blocking its forward path. In the context of this paper, the optimal maneuver for collision avoidance is one that avoids the obstacle from the closest distance, or, equivalently, that minimizes the distance traveled in the current lane. This maneuver is computed by minimizing the longitudinal displacement of the entire lane transition, subject to vehicle dynamics and constraints on the steering angle and the tire forces, as is formulated in the following optimization problem.

4.1 Problem Formulation. Denoting $\mathbf{x} = \{x, \dot{x}, y, \dot{y}, \varphi, \dot{\varphi}\}^T$, and $\mathbf{u} = \{F_t, \beta\}^T$, we solve the following optimization problem:

$$\min_{\mathbf{u}} J = x_1(t_f) = \int_0^{t_f} x_2(\mathbf{x}, \mathbf{u}, t)dt \tag{16}$$

with free final time, t_f, subject to system dynamics

$$\dot{x}_1 = x_2 \tag{17}$$

$$\dot{x}_2 = \frac{1}{m}(u_1 \cos x_5 - F_r \sin x_5 - F_f \sin (x_5 + u_2)) \tag{18}$$

$$\dot{x}_3 = x_4 \tag{19}$$

$$\dot{x}_4 = \frac{1}{m}(F_r \cos x_5 + u_1 \sin x_5 + F_f \cos (x_5 + u_2)) \tag{20}$$

$$\dot{x}_5 = x_6 \tag{21}$$

$$\dot{x}_6 = \frac{1}{I}(-d_r F_r + d_f F_f \cos u_2) \tag{22}$$

the boundary conditions

$$x_1(0) = 0$$

$$x_2(0) = \dot{x}_0$$

$$x_3(t_f) = y_d$$

$$x_4(0) = x_4(t_f) = 0$$

$$x_5(0) = x_6(0) = x_5(t_f) = x_6(t_f) = 0$$

the state constraints

$$h(\mathbf{x}) = F_f(\mathbf{x}) - F_{y\max}(\mathbf{x}) \le 0 \tag{23}$$

and the control constraints

$$g_1(\mathbf{u}) = u_2 - \beta_{\max} \le 0 \tag{24}$$

$$g_2(\mathbf{u}) = \beta_{\min} - u_2 \le 0 \tag{25}$$

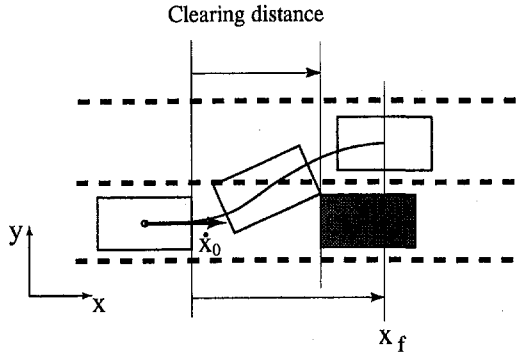

Fig. 3 Lane-change maneuver

$$g_3(\mathbf{x}, \mathbf{u}) = \left(\frac{u_1}{F_{x\max}(\mathbf{x})}\right)^2 + \left(\frac{F_r(\mathbf{x})}{F_{y\max}(\mathbf{x})}\right)^2 - 1 \le 0 \quad (26)$$

$$g_4(u_1) = u_1 - u_{1\max} \le 0 \quad (27)$$

where y_d is the distance between the centers of adjacent lanes, and, using (1), (2), and (14)

$$F_f = -C_f\left(\tan^{-1}\left[\frac{d_f x_6 + x_4 \cos x_5 - x_2 \sin x_5}{x_2 \cos x_5 + x_4 \sin x_5}\right] - u_2\right)$$

$$F_r = -C_r \tan^{-1}\left[\frac{-d_r x_6 + x_4 \cos x_5 - x_2 \sin x_5}{x_2 \cos x_5 + x_4 \sin x_5}\right].$$

where C_f and C_r are the cornering stiffness (C_α) of the front and rear tires, respectively.

The constraint (27) is due to the maximum tractive force, $u_{1\max}$, generated by the maximum engine torque. This constraint applies only to a positive force since the negative force, generated by the brakes, is bounded by the friction ellipse (26).

4.2 Structure of Optimal Control. It is easy to show that the optimal control for this problem is bang-bang in F_t since system dynamics, and hence the Hamiltonian, H, are affine in $u_1 \equiv F_t$:

$$H = x_2 + \lambda_1 x_2 + \lambda_3 x_4 + \lambda_5 x_6 + \left(\frac{\lambda_2}{m}\cos x_5 + \frac{\lambda_3}{m}\sin x_5\right)u_1 + h(\lambda, \mathbf{x}, u_2) \quad (28)$$

where λ_i, $i = 1, \ldots, 6$, are the co-state variables, and $h(\lambda, \mathbf{x}, u_2)$ is a nonlinear function of $\mathbf{x}$ and u_2. Excluding singular arcs, the Hamiltonian (28) is minimized by either maximizing or minimizing u_1. The optimal control is therefore maximum or minimum F_t, subject to constraints (26) and (27). The optimal u_2 (the steering angle) is calculated from $H_{u_2} = 0$. Note that this is also the structure of the equivalent time optimal control problem.

4.3 Trajectory Optimization. A practical solution to the optimization problem (16) is to reformulate it as a parameter optimization. Representing the trajectory, $\mathbf{x}(t)$, by a finite set of parameters, $\mathbf{a} = \{a_1, a_2, \ldots, a_n\}$, transforms (16) to

$$\min_{\mathbf{a}} J = x_1(t_f(\mathbf{a})) \quad (29)$$

subject to the same constraints as (16). Once the optimal trajectory has been found, the optimal controls are computed using inverse dynamics (Shiller and Sundar, 1995).

For the problem treated here, the path is represented by the control points of a cubic B-spline, and the velocity profile along the path is represented by a set of discrete points. The control constraints are appended to the cost function using penalty functions.

Problem (29) can be solved using standard gradient methods. The gradient, though, needs to be computed numerically since the cost function is not explicit in the optimization parameters.

Formulating the optimization problem as a parameter optimization over parameters associated with the trajectory, rather than the controls, was recently introduced by Seywald (1994) as Differential Inclusions, and by Bryson (1995) as Inverse Dynamic Optimization. A similar approach was previously used for optimizing robot motions (Shiller and Dubowsky, 1989).

This optimization scheme is computationally more efficient than traditional variational methods since it does not require co-states, state constraints can be easily considered (transformed to constraints on the parameters), and boundary conditions are easily satisfied. In addition, this optimization scheme can be terminated (if computation time is bounded) to produce suboptimal but feasible solutions, which is not the case with variational methods that must satisfy necessary optimality conditions (Bryson and Ho, 1975).

The optimal trajectories can be used as reference trajectories for on-line feedback controllers, or to determine the minimum *clearing distance,* the distance beyond which an obstacle cannot be avoided for given initial speeds, as discussed next.

5 Minimum Clearing Distance

The minimum *clearing distance*, $x_c(\dot{x}_0)$, is defined as:

$$x_c(\dot{x}_0) = \min_t x(\dot{x}_0, t) \quad (30)$$

where $x(\dot{x}_0, t)$ is the optimal trajectory, subject to the condition

$$A(t, \dot{x}_0) \cap B(x) = 0, \quad t \in [0, t_f], \quad x > 0 \quad (31)$$

where x is the distance between the vehicle and obstacle, $A(t, \dot{x}_0)$ represents the volume swept by the moving vehicle along the optimal trajectory at time t, and $B(x)$ represents the volume occupied by the static obstacle, positioned in the current lane at a distance x from the vehicle when it begins the lane-change maneuver.

The minimum *clearing distance* can be computed by determining the point at which a vertex of the vehicle moving along the optimal trajectory intersects a vertex of the static obstacle, as shown in Fig. 4.

For a left lane transition, the points of concern are the front right corner of the moving vehicle and the rear left corner of the obstacle. Let the optimal trajectory be $\mathbf{x}(\dot{x}_0, t) = \{x(\dot{x}_0, t), y(\dot{x}_0, t), \varphi(\dot{x}_0, t)\}$. Then, the time, t_c, at which the two vertices coincide is the time when the y coordinate of the front right corner of the vehicle passes through $y = b/2$ (assuming the vehicle and obstacle are of identical geometries):

$$y(t_c, \dot{x}_0) + d_f \sin \varphi(t_c, \dot{x}_0) - \frac{b}{2}\cos \varphi(t_c, \dot{x}_0) = \frac{b}{2} \quad (32)$$

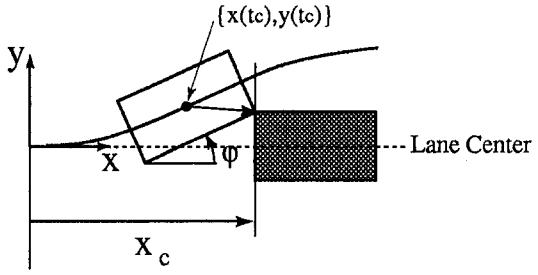

Fig. 4 Calculating the minimum clearing distance

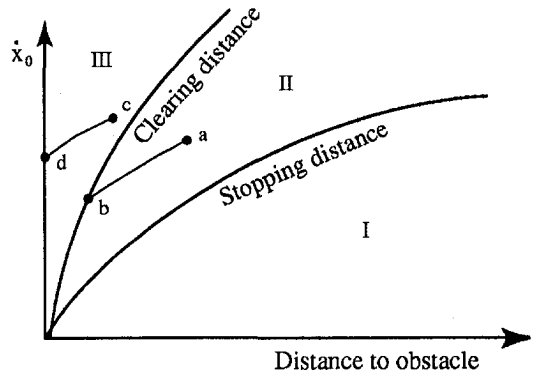

Fig. 5 The clearance curve in the phase-plane

The minimum clearing distance, $x_c(\dot{x}_0)$, is then

$$x_c(\dot{x}_0) = x(t_c, \dot{x}_0) + d_f \cos \varphi(t_c) + \frac{b}{2} \sin \varphi(t_c) \quad (33)$$

where b is the vehicle's width.

Plotting $\dot{x}_0$ versus $x_c(\dot{x}_0)$ for the optimal maneuvers, computed for various initial speeds, produces the clearance curve in the phase plane $\dot{x} - x$, as shown schematically in Fig. 5. The clearance curve marks the boundary of the vehicle's states (position and speed) from which an obstacle can be avoided. States right of the curve are avoidable, whereas states left of the curve are not.

It is useful to add the stopping curve, representing states from which the vehicle can decelerate to a full stop and just touch the obstacle, using the maximum deceleration, as shown schematically in Fig. 5. The *stopping* curve is simply computed by:

$$\dot{x} = \sqrt{2\ddot{x}_{\min} x} \quad (34)$$

where $\ddot{x}_{\min}$ is the maximum longitudinal deceleration, which depends on the vehicle weight and road conditions.

These curves can assist in planning an avoidance maneuver. For example, detecting the obstacle at a speed and distance corresponding to Region I, leaves sufficient time for a full stop, or for a relaxed[1] lane transition. Detecting the obstacle in Region II (for example, point a) leaves a lane transition or a head-on collision as the only options. An avoidance maneuver in Region II may consist of a relaxed maneuver from point a. Alternatively, the avoidance maneuver may consist of a deceleration, until hitting the clearance curve, then an optimal maneuver corresponding to a lower speed (point b). The preferred maneuver depends on the congestion in the neighboring lanes. First decelerating and then executing the optimal maneuver would allow the longest time in the current lane. Crossing the clearance curve into Region III (for example, point c) eliminates the lane-change option. The best strategy then is to stay in the current lane, decelerate at the maximum deceleration, and brace for a head-on collision at a lower speed (point d). Attempting a lane transition from points in Region III may result in an off-center collision, or loss of control. Either is generally more dangerous than a head-on collision, for which the vehicle is better designed to sustain.

In addition to assisting in planning collision-avoidance maneuvers, the clearance curve can be used to specify the minimum range of collision-avoidance sensors. Clearly, any collision-avoidance sensor must have a minimum range outside of Region III. Yet another potential use of the clearance curve is to provide a unified metric for comparing between the dynamic performance of different vehicles. The slope of the curve represents a measure of the vehicle's ability to sustain sharp turns at high speeds: the steeper the better.

[1] In the context of this paper, a relaxed maneuver is one that satisfies criteria not essential for safety, such as ride comfort.

6 On-Line Approximations of Emergency Maneuvers

Computing the clearance curve using the optimal maneuvers is computationally too expensive for on-line applications. It can be approximated using a simple point mass model. While this may not produce the optimal maneuvers, it can account for the actual vehicle parameters and changing road conditions.

6.1 The Point Mass Model. The point mass model consists of a point mass, forced by two independent perpendicular forces, as shown in Fig. 6. The optimal lane-change maneuver for this system is computed by solving the following optimization problem

$$\min J = x(t_f) \quad (35)$$

where t_f is free, subject to system dynamics

$$\ddot{x}(t) = \frac{F_x}{m} \quad (36)$$

$$\ddot{y}(t) = \frac{F_y}{m} \quad (37)$$

the control constraints

$$|F_x| \le F_{x\max} \quad (38)$$

$$|F_y| \le F_{y\max} \quad (39)$$

and boundary conditions

$$\dot{x}(0) = \dot{x}_0 \quad (40)$$

$$\dot{x} = \text{free} \quad (41)$$

$$y(0) = x(0) = 0, \quad (42)$$

$$y(t_f) = y_d, \quad (43)$$

$$\dot{y}(0) = \dot{y}(t_f) = 0 \quad (44)$$

where y_d is the distance between the centers of adjacent lanes.

Problem (35) consists of two separate problems coupled only by the boundary conditions. The first problem is to minimize the motion distance in the x direction for $t \in [0, t_f]$. The second is to determine the final time, t_f, from the motion in the y direction. Since x_f is minimized if t_f is minimized (assuming $\dot{x} > 0$), the motion in the y direction should be of minimum time.

The optimal control in the y direction is, therefore, bang-bang with one switch at $t = (t_f/2)$. The motion in the x direction minimizes x_f, which is equivalent to minimizing $\dot{x}$:

$$\min J = x(t_f) = \int_0^{t_f} \dot{x} dt \quad (45)$$

It is easy to show that the optimal control for problem (45) is the maximum braking force.

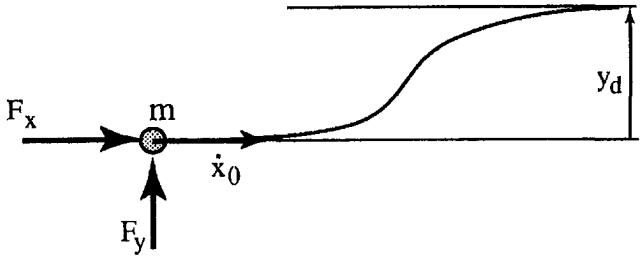

Fig. 6 The point mass model

Integrating the optimal control twice with respect to time yields analytical expressions for $x(t)$ and $y(t)$ as functions of the initial speed $\dot{x}_0$, the vehicle mass, m, and the actuator constraints:

$$x(t) = \dot{x}_0 t - \frac{1}{2}\frac{F_{x\max}}{m} t^2 \tag{46}$$

$$y(t) = \begin{cases} \frac{1}{2}\frac{F_{y\max}}{m} t^2, & 0 < t < \frac{t_f}{2} \\ 2\sqrt{y_d \frac{F_{y\max}}{m}}\, t - \frac{1}{2}\frac{F_{x\max}}{m} t^2 - y_d, & \frac{t_f}{2} < t \le t_f \end{cases} \tag{47}$$

where

$$t_f = 2\sqrt{\frac{m y_d}{F_{y\max}}} \tag{48}$$

$$x_f = \dot{x}_0 t_f - \frac{1}{2}\frac{F_{x\max}}{m} t_f^2 \tag{49}$$

It is assumed that $\dot{x}(t) > 0$ for all $t \in [0, t_f]$. To ensure forward motion ($x_f > 0$), we may restrict the initial speed or reduce $F_{x\max}$ so that

$$\dot{x}_0 > \frac{F_{x\max}}{m} t_f \tag{50}$$

The optimal maneuvers for the point mass model can be easily computed using (46) and (47) for any given initial speed. The actuator limits, $F_{x\max}$ and $F_{y\max}$, can be chosen as the major axes of the friction ellipse (15), or more conservatively to ensure that the resulting maneuver is dynamically feasible. The smaller the force limit, the longer the maneuver.

6.2 The Clearance Curve. To approximate the clearance curve, we translate the trajectory by d_f and $-b/2$ in the x and y directions, respectively, solve for the time at which the y trajectory passes through $b/2$ using (47), then substitute this time in (46) to yield the relations between the clearing distance and the initial speed:

$$x_c(\dot{x}_0) = \dot{x}_0 \sqrt{\frac{2bm}{F_{y\max}}} - \frac{bF_{x\max}}{F_{y\max}} + d_f \tag{51}$$

Rewriting (51) yields the equation for the clearance curve:

$$\dot{x}_0 = \sqrt{\frac{F_{y\max}}{2bm}}\, x_c + \frac{bF_{x\max}}{F_{y\max}} - d_f \tag{52}$$

It is a straight line in the phase-space $x_c - \dot{x}_0$. This line does not pass through the origin due to the offset caused by the vehicle size (the obstacle cannot be avoided at a close range regardless of speed). This offset, however, is of the order of magnitude of the vehicle width, and can be practically ignored.

The clearance curve can be characterized by its slope $\sqrt{F_{y\max}/2bm}$. But the slope is inversely proportional to the time to collision from the last point a lane-change maneuver is feasible (assuming the curve passes through the origin). The time to collision, t_c, is thus:

$$t_c = \sqrt{\frac{2bm}{F_{y\max}}} \tag{53}$$

For the point mass model, this time is fixed for all initial speeds. It increases with the vehicle mass and decreases with the magnitude of the side tire force (the vehicle's cornering ability), as expected. The time to collision can serve as an alternative criterion for deciding when to, or not to, change lane: a lane change maneuver is feasible when $t \ge t_c$, and infeasible otherwise.

Table 1 Parameters of the planar vehicle

b [m]	$d_f = d_r$ [m]	m [Kg]	I [Kg − m^2]	C_r [N/rad]	C_f [N/rad]
2	2	1,550	3,100	80,000	80,000
α^*	β_{max}	F_{tmax} [N]	F_{tmin} [N]	F_{xmax} [N]	F_{ymax} [N]
5°	50°	3,000	−6,000	6,000	5,000

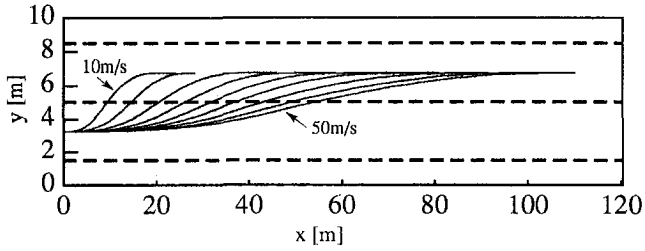

Fig. 7 Optimal lane change maneuvers

7 Examples

The optimization of the lane-change maneuvers was implemented on a Silicon Graphics workstation for the planar bicycle model, using the parameters of a medium size passenger car given in Table 1. The following examples provide some insights into the general shapes of the optimal emergency maneuvers for the bicycle and the point mass models, in addition to presenting the clearance curves associated with these maneuvers.

7.1 Optimal Maneuvers. Using 12 control points to represent the path, and 7 points to represent the velocity profile, resulted in the optimal maneuvers shown in Fig. 7. As is evident from Fig. 7, the higher the speed, the longer the maneuver. The duration of these maneuvers, though, changed little with the initial speeds (2.6 s at 20 m/s to 2.3 s at 50 m/s). The optimal velocity profiles for these maneuvers are shown in Fig. 8. The active constraint in all optimal maneuvers was the friction ellipse (26).

Figure 9 shows the optimal steering angles along three maneuvers, normalized with respect to the total path distance. Generally, the higher the speeds, the smaller and more oscillatory the steering angle. This suggests that the sinusoidal steering

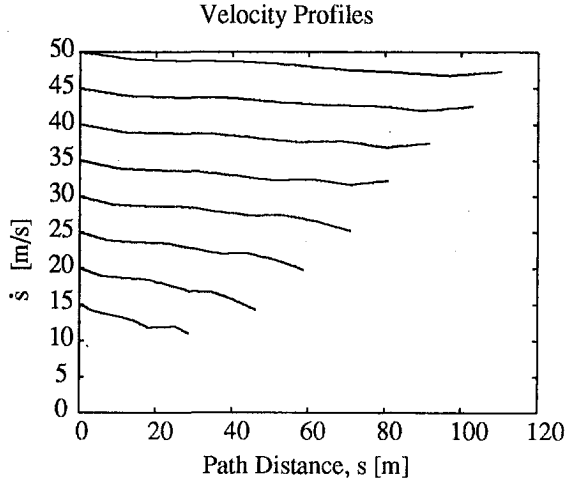

Fig. 8 Velocity profiles along optimal lane change maneuvers

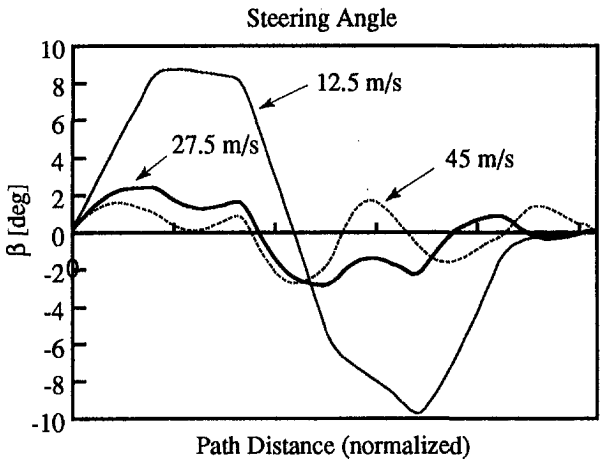

Fig. 9 Steering angle along optimal maneuvers

inputs, commonly used in the literature for lane change maneuvers, are inadequate for emergency maneuvers at high speeds.

Figure 10 shows the clearance curve for the optimal maneuvers shown in Fig. 7. It is roughly a straight line (the slight deviations may be due to small numerical errors). This line was computed for maneuvers from 50 m/s down to 10 m/s. It was extrapolated for lower speeds, as shown by the dashed line in Fig. 10. The slope of this line is close to 1 s^{-1}, suggesting $t_c = 1$ s, the time to collision when the obstacle must be avoided using the optimal maneuver. This result reflects the specific parameters used in our model. It is remarkably close to the experimental results of 1 s to collision (regardless of speed) obtained independently at Honda Motors for a a medium size passenger car (similar to ours) (Fujita et al., 1994).

Although this comparison is inconclusive due to the lack of data on the experimental vehicle, the closeness of these results confirms the validity of our approach.

The clearance curve is significantly different from the hyperbolic stopping curve shown in Fig. 10 for the maximum braking deceleration of $\ddot{x}_{min} = 3.87$ m/s^2. The difference between the two curves clearly demonstrates the advantage of lane-change maneuvers over a full stop at high speeds. For example, a vehicle traveling at 30 m/s (108 Km/h) requires 116 m for a full stop, whereas it requires only 30 m for an optimal lane-change maneuver. The higher the speed, the larger the difference.

The time in the current lane may be maximized by decelerating as soon as the obstacle is detected, until reaching the clearance curve at a lower speed. For example, detecting the obstacle

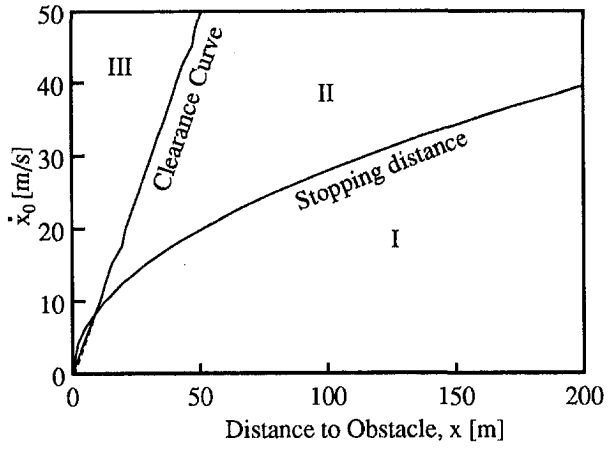

Fig. 10 The clearance curve for the optimal maneuvers of Fig. 5

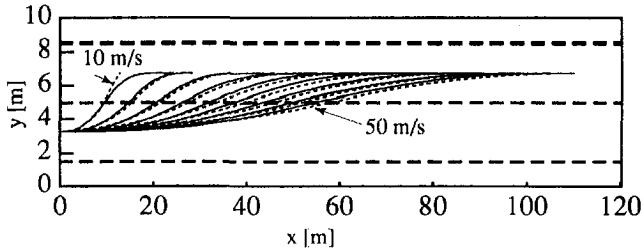

Fig. 11 Optimal (solid) and approximated (dashed) maneuvers

from a distance of 80 m at 30 m/s (leaving no option for a full stop) and maintaining the current speed would allow 1.6 s before the vehicle must execute an optimal maneuver. Decelerating at the maximum deceleration would extend the time in the current lane to 2.3 s before reaching the clearance curve at 21 m/s, an increase of 40 percent. The extra time can be used for communication with the neighboring vehicles and coordination of the lane transition.

7.2 Point Mass Model. Computing the optimal maneuvers for the point mass model, using the major axes of the friction ellipse (15) as the force limits, resulted in the approximated maneuvers shown in Fig. 11. These maneuvers are very close to the optimal maneuvers computed for the nonlinear bicycle model. The velocity profiles of the point mass model are steeper (higher deceleration) than those for the bicycle model, as can be seen in Fig. 12.

It is interesting to compare the total motion times for the optimal and the approximated maneuvers. For the approximated maneuvers, it is constant, at 2.08 s, independently of the initial speed, whereas for the optimal maneuver it varies little from 2.3 for 50 m/s to 2.6 s for 20 m/s. The optimal maneuvers take slightly longer due to the lower deceleration during the turns. The point mass model can thus be used to closely approximate the paths of the lane change maneuvers. The velocity profile along the path can be computed using the method presented in (Shiller and Sundar, 1995), which is generally simpler and computationally more efficient than the optimization of the entire maneuver.

The clearance curve for the point mass model is a straight line, as discussed earlier. For the parameters used, the slope of this line is 0.9 s^{-1}, almost overlapping with the line shown in Fig. 10. Consequently, the time to collision on the clearance curve, t_c, is (53) $t_c = \sqrt{2*2*1550/5{,}000} = 1.1$ s, very similar

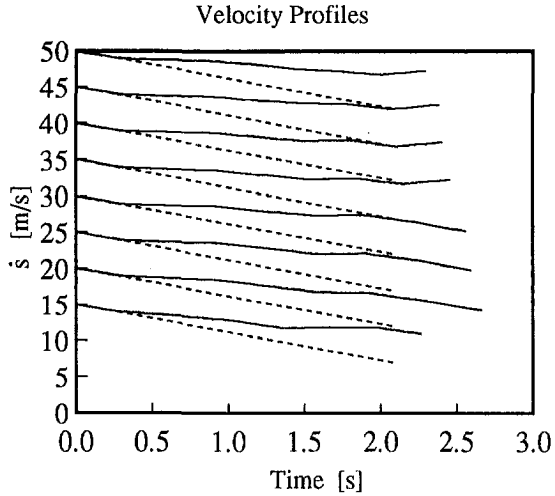

Fig. 12 Velocity profiles of optimal (solid) and approximated (dashed) maneuvers

to the experimental results (Fujita et al., 1994). This strongly suggests the point mass model as an excellent candidate for estimating the clearance curve and for approximating emergency lane-change maneuvers.

8 Conclusions

This paper addresses the issue of emergency lane-change maneuvers for obstacle avoidance. We first characterize an emergency lane-change maneuver as a maneuver that minimizes the longitudinal distance of the lane transition. This maneuver is the sharpest possible (consisting of the tightest curves) as it slides along the tire force constraints. It therefore determines the last point at a given speed from which the obstacle is avoidable. This is critical for planning lane-change maneuvers since attempting a maneuver beyond this "last" point would result in an off-center collision, which is generally more dangerous than a head-on collision at the same speed.

A procedure for computing optimal maneuvers for a bicycle model is also presented. It is shown that the shape of the optimal maneuver depends primarily on the initial speed: the faster the longer, whereas the duration of the maneuvers varies little with speed. Computing the optimal maneuvers for various speeds allows to generate the clearance curve, which depicts the distance to the closest avoidable obstacle as a function of speed. For the bicycle model, the clearance curve is shown to be almost linear with respect to the initial speed for the optimal maneuvers, compared to the hyperbolic curve for the distance to a full stop. This clearly demonstrates the advantage of lane change maneuvers over a full stop at high speeds.

The clearance curve was shown as a valuable design tool for planning safe avoidance maneuvers. It allows to maximize the time from the detection of the obstacle to the time when a lane change maneuver must be executed, as was demonstrated in the examples. The clearance curve can also be used as a benchmark for evaluating other avoidance maneuvers, or as a unified measure of the dynamic performance of different vehicles: the safest vehicle is the one with the steepest slope.

On-line computation of emergency maneuvers was also presented, using a simple point mass model. It is computationally very efficient as it yields an analytical solution, and is shown to closely approximate the paths and the clearance curve of the optimal maneuvers. The examples for both the bicycle and the point mass models were remarkably close to the experimental results reported by Honda Motors for a similar vehicle.

Acknowledgments

The support of the California State Department of Transportation through the Program on Advanced Technology for the Highway (PATH) is acknowledged. Part of this work was performed at the Commotion (Cooperative Motion) Laboratory at UCLA, which has been supported by NSF Grant CDA-9303148.

The first author would also like to thank Mr. Furukawa and his colleagues of the Intelligent Vehicle group at Honda R&D Co., Tochigi R&D Center, Japan, for insightful discussions and for sharing their experimental results on obstacle avoidance.

References

Bryson, A., 1995, "Inverse Dynamic Optimization," MANE Seminar, UCLA, April.

Bryson, A. E., and Ho, Y. C., 1969, *Applied Optimal Control,* Blaisdell Publishing Company.

Chee, W., and Tomizuka, M., 1994, "Lane Change Maneuver of Automobiles for the Intelligent Vehicle and Highway System (IVHS)," American Control Conference, June, pp. 3586–3587.

Dugoff, H., P. S. Fancher, and L. Segel, 1970, "An Analysis of Tire Properties and Their Influence on Vehicle Dynamics Performance," *SAE Transactions* 700377.

Fiorini, P., and Shiller, Z., 1998, "Motion Planning in Dynamic Environments using Velocity Obstacles," to appear in *International Journal of Robotics Research.*

Fujita, Y., K. Akuzawa, and M. Sato, 1994, "Radar Brake System," AVEC 1994, No. 9438583.

Gim, G., and P. E. Nikravesh, 1991, "An Analytical Model of Pneumatic Tires for Vehicle Dynamic Simulations. Part 3: Validation Against Experimental Data." *Int. J. of Vehicle Design,* Vol. 12, No. 2, pp. 217–228.

Maalej, A. Y., Guenther, D. A., and Ellis, J. R., 1989, "Experimental Development of Tire Force and Moment Models," *International Journal of Vehicle Design,* Vol. 10, No. 1, pp. 34–50.

Narendran, V. K., and Hedrick, J. K., 1993, "Transition Maneuvers in Intelligent Vehicle Highway Systems," *Proc. of Conference on Decision and Control,* San Antonio, TX, Dec., pp. 1880–1884.

Sakai, H., 1981, "Theoretical and Experimental Studies on the Dynamic Properties of Tires," *International Journal of Vehicle Design,* Vol. 2, No. 1.

Seywald, H., 1994, "Trajectory Optimization Based on Differential Inclusion," *AIAA Journal of Guidance, Control and Dynamics,* Vol. 17, No. 3.

Shiller, Z., and Dubowsky, S., 1989, "Time Optimal Path Planning for Robotic Manipulators with Obstacles, Actuator, Gripper and Payload, Constraints," *Int'l J. Robotics Research,* Vol. 8, No. 6, Dec., pp. 3–18.

Shiller, Z., and Sundar, S., 1995, "Emergency Maneuvers of AHS Vehicles," SAE 1995 Transactions. *Journal of Passenger Cars,* Section 6, Vol. 104 paper 951893, pp. 2633–2643.

Smith, D. E., and Starkey, J. M., 1994, "Effects of model complexity on the performance of automated vehicle steering controller: controller development and evaluation," *Journal of Vehicle System Dynamics,* Vol. 23, pp. 627–645.